HEP-14-0077

Supporting Materials and Methods

Zebrafish lines

Zebrafish embryos, larvae, and adult fish were raised under standard laboratory conditions at 28°C (1). The following wild-type and transgenic lines were used: AB/TL, AB, *Tg(fabp10a:CFP-Eco.NfsB)*^{gt1}, *Tg(fabp10a:mCherry-Eco.NfsB)*^{gt2}, *Tg(fabp10a:dsRed;ela3l:EGFP)*^{gz15} (2), *Tg(-2.8fabp10a:EGFP)*^{as3} (3), *Tg(EPV.Tp1-Ocu.Hbb2:hmgb1-mCherry)*^{jh11} (4), *Tg(EPV.Tp1-Mmu.Hbb:EGFP)*^{um14} (4), *Tg(kdrl:EGFP)*^{s843} (5), *TgBAC(hand2:EGFP)*^{pd24} (6), *Tg(EPV.Tp1-Ocu.Hbb2:CreERT2)*^{jh12} (7), *Tg(actb2:loxP-STOP-loxP-hmgb1-mCherry)*^{jh15} (7), *Tg(EPV.Tp1-Mmu.Hbb:hist2h2l-mCherry)*^{s939} (8), *Tg(EPV.Tp1-Mmu.Hbb:Venus-Mmu.Odc1)*^{s940} (8), *Tg(-1.5hsp70l:Gal4)*^{kca4} (9), *Tg(5xUAS-E1b:6xMYC-notch1a)*^{kca3} (10), *Tg(hsp70l:wnt8a-GFP)*^{w34} (11), and *Tg(hsp70l:Mmu.Axin1-YFP)*^{w35} (12). The transgenic lines are abbreviated as *Tg(fabp10a:CFP-NTR)*^{gt1}, *Tg(fabp10a:mCherry-NTR)*^{gt2}, *Tg(fabp10a:dsRed;ela3l:EGFP)*^{gz15}, *Tg(fabp10a:EGFP)*^{as3}, *Tg(Tp1:mCherry)*^{jh11}, *Tg(Tp1:EGFP)*^{um14}, *Tg(kdrl:EGFP)*^{s843}, *Tg(hand2:EGFP)*^{pd24}, *Tg(Tp1:CreERT2)*^{jh12}, *Tg(actb2:loxP-STOP-loxP-mCherry)*^{jh15}, *Tg(Tp1:H2BmCherry)*^{s939}, *Tg(Tp1:VenusPEST)*^{s940}, *Tg(hs:Gal4)*^{kca4}, *Tg(UAS:MYC-notch1a)*^{kca3}, *Tg(hs:wnt8a-GFP)*^{w34}, and *Tg(hs:Axin1)*^{w35}, respectively.

Nitroreductase constructs

To express CFP or mCherry-NTR fusion protein in hepatocytes, a 2.8kb fragment of the zebrafish hepatocyte-specific *fatty acid binding protein 10a, liver basic* promoter was cloned into a modified version of pBluescriptII SK+ with I-SceI restriction sites (13). Each plasmid was injected into a one-cell stage embryo along with I-SceI meganuclease (14). *Tg(fabp10a:CFP-NTR)*^{gt1} and *Tg(fabp10a:mCherry-NTR)*^{gt2} adult carriers were identified by screening their progeny for CFP or mCherry fluorescence.

Heat shock and genotyping

Heat shock regimens were as follows: before MTZ treatment, 80 hpf, 39°C for 1 hour; after MTZ treatment, 2 hpa, 39°C for 40 minutes. *Tg(hs:wnt8a-GFP)*^{w34} and *Tg(hs:Axin1-YFP)*^{w35} larvae were sorted based on their expression of GFP and YFP, respectively, 3 hours after heat shock. [*Tg(hs:Gal4)*^{kca4}*; Tg(UAS:MYC-notch1a)*^{kac3}*; Tg(Tp1:mCherry)*^{jh11}] larvae were sorted based on their upregulation of mCherry expression at 0 hpa.

Tissue preparation and immunohistochemistry

Dissected adult livers and larvae were fixed with 2% formaldehyde in 0.1 M PIPES, 1.0 mM $MgSO_4$, and 2 mM EGTA overnight at 4°C. Prior to immunohistochemistry, yolk and skin of larvae were manually removed. Adult livers were cut into 50µm sections using VT1000S vibratome (Leica Biosystems, Germany). Liver sections and larvae were then blocked with 4% BSA, 0.3% Triton X-100 in PBS overnight at 4°C. Primary and secondary antibody staining were performed overnight at 4°C. We used the following antibodies: mouse monoclonal anti-Alcam/Zn8 (1:15; ZIRC), rabbit polyclonal

anti-Laminin (1:100; Sigma-Aldrich, St. Louis, MO) and anti-type I Collagen (1:100; Abcam, Cambridge, MA), and fluorescently conjugated secondary antibodies from Molecular Probes (1:200; Carlsbad, CA).

5-Ethynyl-2'-Deoxyuridine (EdU) cell cycle analysis

To assess cell proliferation, animals were incubated with 7μM 5-Ethynyl-2'-Deoxyuridine (EdU) and DMSO at 1.7% final concentration for the indicated time point. EdU incorporation was revealed for 30 minutes using Click-iT EdU Imaging Kit (Invitrogen, Carlsbad, CA).

Tamoxifen and LY411575 treatment

To perform genetic inducible fate mapping, zebrafish larvae were treated with 5μM 4-Hydroxytamoxifen (4-OHT, Sigma-Aldrich, St. Louis, MO) to induce Cre-recombinase at the indicated developmental stages. To inhibit Notch signaling, larvae were incubated with 10μM LY411575 (Stemgent, Cambridge, MA) at the stages indicated.

PED6 assay

PED6 assay was performed as previously described (15). Wild type and regenerating larvae were soaked with 0.3μg/ml PED6 in embryo medium for 4 hours and epifluorescence live images were then taken by the Leica M205 FA fluorescence stereo microscope (Leica Biosystems, Germany).

Confocal imaging and quantification of cell numbers

Confocal images were obtained using a Zeiss LSM510 VIS or LSM700 confocal microscope. The whole liver area was scanned using Z stack. To quantify the number of cells, cells in 5 planes at 5μm intervals were counted for each sample. Cells were counted using the cell counter tool in ImageJ (National Institutes of Health, Bethesda, MD). Cell numbers were counted in more than 6 larvae for each sample.

Western blot analysis

Livers from 100 larvae and individual adult fish were dissected and extracted in RIPA buffer (50 mM Tris-HCl, pH 8.0, 150 mM sodium chloride, 1% NP-40, 0.5% sodium deoxycholate, 0.1% SDS, 2 mM EDTA and 1 mM PMSF) with Protease inhibitor cocktail (Sigma-Aldrich, St. Louis, MO). Proteins were separated on 6% SDS-PAGE gels and transferred to Hybond-ECL nitrocellulose membranes (GE Healthcare, Pittsburgh, PA). The membranes were incubated with rabbit polyclonal anti-Laminin (1:1000; Sigma-Aldrich, St. Louis, MO), anti-β-actin (1:1000; Cell Signaling Technology, Beverly, MA) or anti-type I Collagen (1:100; Abcam, Cambridge, MA) antibody. The blots were subsequently incubated with horseradish peroxidase-conjugated secondary antibodies and visualized using commercial ECL kits (Pierce Biotechnology Inc., Rockford, IL).

Quantitative real-time polymerase chain reaction

The livers of 50 DMSO-treated (7 dpf) and MTZ-treated (0 and 1 dpa) larvae with or without 1.5% EtOH and with or without Wnt agonists were dissected. RNA was extracted using the Trizol Reagent (Invitrogen, Carlsbad, CA) according to the

manufacturer's instruction. cDNA synthesis was performed using Superscript III First-strand Synthesis System (Invitrogen, Carlsbad, CA). PCR was conducted using iTaq Universal SYBR Green Supermix in triplicate (Bio-Rad, Hercules, CA). Optimized primers targeting each gene were designed using Primer3 (16). The StepONE Plus PCR System (Applied Biosystems, Carlsbad, CA) was used to obtain the *C*t value. The relative gene expression of each sample was determined using the comparative *C*t method with *β-actin* as an internal control (17). Results from at least three independent experiments were shown. The primers used include: *hes1b* forward, 5'-AAGCTTGGGTCAGCTGAAAA-3'; *hes1b* reverse, 5'-GAACGGTGGGATCTGTGTTT-3'; *numb* forward, 5'-GCTGAAGACGGACAGAAAGG-3'; *numb* reverse, 5'-GCGCACAGAAAGAAACCTTC-3'; *β-actin* forward, 5'-CGAGCTGTCTTCCCATCCA-3'; *β-actin* reverse, 5'-TCACCAACGTAGCTGTCTTTCTG-3'; *col1a1a* forward, 5'-AAGGAGGGCCAGAAAGGTAA-3'; *col1a1a* reverse, 5'-TACCACGCTGACCACCAATA-3'; *col1a2* forward, 5'-GCATGAAGGGACACAGAGGT-3'; *col1a2* reverse, 5'-CGACCTCTCTCACCAGGAAG-3'.

Reporter assay

Luciferase assays in HEK293T cells were performed in 24-well plates in triplicates. Cells were transfected with Lipofectamine 2000 (Invitrogen, Carlsbad, CA) according to manufacturer's protocol. The plasmid concentrations used include (ng per well):

pTOPflash, 150 ng; pCMV-Renilla, 10 ng; phosphorylated β-catenin-Y33, 450 ng. *Firefly* luciferase and *renilla* activities were measured using the dual luciferase assay kit (Promega, Madison, WI). *Firefly* luciferase activity was normalized against *renilla* activity.

Statistical analysis

The *p*-values were calculated using an unpaired two-tailed Student *t*-test with Excel (Microsoft, Redmond, WA).

Chemical screens

To perform chemical screens for compounds enhancing hepatocyte regeneration, we tested 75 compounds from the Stem Cell Signaling Compound Library (Selleckchem, Houston, TX) and 1,000 compounds from the ActiProbe-1K Library (TimTec, Newark, DE). We aliquoted each chemical compound into two separate wells of a 96-well glass bottom microwell plate (Matrical Bioscience, Spokane, WA) to a final concentration of 50 mM. Control larvae were treated with equal concentrations of DMSO in embryo medium. For the Stem Cell Signaling Compound Library, both EtOH/MTZ-treated and MTZ-treated [*Tg(fabp10a:CFP-NTR)*^{gt1}*; Tg(Tp1:VenusPEST)*^{s940}] larvae were used, while for the ActiProbe-1K Library, only MTZ-treated larvae were used for the initial screens. Three to five ablated larvae were pipetted into each well. At 40-50 hpa, the number and intensity of CFP-positive cells within each larval liver were determined using a Leica M205 FA fluorescence microscope. 16 compounds from the ActiProbe-1K Library and 9 compounds from the Stem Cell Signaling Compound Library (Supporting

Table 1) that changed the number and/or intensity of CFP-positive cells within the liver in at least two embryos in both wells were retested at a range of concentrations from 10-100 mM. Two of the compounds, [bisbenzyldimethylamine, chloride] and [4-(1H-1,2,3,4-tetraazol-5-yl)-1,2,5-oxadiazole-3-ylamine] taken from the ActiProb-1K Library showed a significant enhancement in Topflash reporter activity. Two Wnt agonists, SB 415286 and CHIR-99021 taken from the Stem Cell Signaling Compound Library showed higher efficiency in hepatocyte regeneration at 25mM or lower concentrations than other Wnt agonists on retesting. These four compounds were further evaluated by examining the MTZ/DMSO-treated, MTZ/compound-treated, and EtOH/MTZ/compound-treated regenerating livers in [*Tg(fabp10a:CFP-NTR)*^{gt1}*; Tg(Tp1:mCherry)*^{jh11}] larvae with confocal microscopy and counting the number/percentage of the HPCs in each condition as described in the Supporting Materials and Methods section.

Supporting Figure Legends

Supporting Fig. 1. Establishing a hepatocyte-specific genetic ablation system. (A-A'', B, E-E'' and F) DMSO-treated livers at 5 days-post-fertilization (dpf). (C-C'', D, G-G'' and H) MTZ-treated livers at 0 hours-post-ablation (hpa). (A-A'') Expression of *Tg(fabp10a:*mCherry-NTR) (A, A') and *Tg(fabp10a:*EGFP) (A, A'') mark hepatocytes in control larvae. (B) *Tg(Tp1:*EGFP) marks the cell bodies and cytoplasmic extensions of Notch-responsive cells (NRCs). (C-C'') MTZ induced significant reduction of *Tg(fabp10a:*mCherry-NTR) (C, C') and *Tg(fabp10a:*EGFP) (C, C''). (D) MTZ treatment resulted in near complete destruction of hepatocytes with collapsed cell bodies and cytoplasmic extensions of NRCs. (E-E'') Expression of *Tg(fabp10a:*CFP-NTR) (E, E') and *Tg(fabp10a:*dsRed) (E, E'') mark hepatocytes in control larvae. (F) Hepatocytes express *Tg(fabp10a:*CFP-NTR), while the nuclei of NRCs are indicated by the expression of *Tg(Tp1:*mCherry). (G-G'') MTZ-treated larvae showed nearly complete absence of *Tg(fabp10a:*CFP-NTR) (G, G') and *Tg(fabp10a:*dsRed) (G, G''). (H) NRCs became clustered together with the ablation of hepatocytes. MTZ-treated larvae were sorted based on the criteria of complete absence of hepatocyte-specific fluorescence and significantly reduced liver volume indicated by clustered NRCs. A-A'', C-C'', E-E'' and G-G'', fluorescent images or combined with bright-field images (n=90 larvae per condition in three experiments). B, D, F and H, confocal images (n=30 larvae per condition in three experiments). Scale bars: A-A'', C-C'', E-E'' and G-G'', 100μm; B, D, F and H, 20μm.

Supporting Fig. 2. Establishing an ablation system that permits the targeted destruction of hepatocytes. (A-C) Control [*Tg(fabp10a:mCherry-NTR)*^{gt2}; *Tg(Tp1:EGFP)*^{um14}] (A),

[*Tg(fabp10a:mCherry-NTR)*^{gt2}; *Tg(kdrl:EGFP)*^{s843}] (B) and [*Tg(fabp10a:mCherry-NTR)*^{gt2}; *TgBAC(hand2:EGFP)*^{pd24}] (C) livers treated with DMSO. (D-F) MTZ-treated livers are outlined with white dotted lines at 0 hpa. Larvae treated with MTZ showed intact NRCs (D), endothelial cells (E) and HSCs (F), whereas there was a significant or complete loss of hepatocytes. A-C, confocal single-plane image; D-F, confocal projection images (n=30 larvae per condition in three experiments). Scale bar, 20μm.

Supporting Fig. 3. Increased deposition of fibrillar type I collagen in the EtOH/MTZ-treated regenerating livers. (A-A’’’) In [*Tg(fabp10a:CFP-NTR)*^{gt1}; *Tg(Tp1:mCherry)*^{jh11}; *Tg(hand2:EGFP)*^{pd24}] larvae treated with DMSO at 5 dpf, quiescent HSCs showed a star-shaped configuration (A’, inset), whereas fibrillar type I collagen was almost undetectable (A’’) and NRCs distributed among hepatocytes (A, A’’’). (B-B’’’) Hepatocytes were ablated by MTZ and allowed to regenerate for 50 hours. In the MTZ-treated regenerating livers, the number of HSCs increased (B’) with a rare deposition of type I collagen (B’’). A population of cells co-expressing hepatocyte-specific CFP and NRC-specific nuclear mCherry was observed throughout the MTZ-treated regenerating livers (B’’’, inset, white arrows) while bright red NRCs remained CFP negative (B’’’, inset, yellow arrowhead). (C-C’’’) The larvae were pretreated with 1.5% EtOH from 2.5 to 3.5 dpf and then concurrently treated with MTZ from 3.5 to 4.5 dpf and allowed to regenerate for 50 hours. HSCs increased in number and showed less complex cytoplasmic processes (C’, inset). Elevated type I collagen deposition was observed in the EtOH/MTZ-treated livers (C’’, inset). A population of

cells co-expressing hepatocyte-specific CFP and NRC-specific nuclear mCherry was detected (C’’’, inset, white arrows) while bright red NRCs remained CFP negative (C’’’, inset, yellow arrowhead). (D) qRT-PCR analysis showed upregulation of *collagen 1a1a* and *collagen 1a2* mRNA in the EtOH/MTZ-treated regenerating livers. n=150 dissected larval livers per condition in three experiments. Asterisks indicate statistical significance: **p*<0.05 and ***p*<0.01. (E) Percentage (mean±SD) of CFP^+ cells in the population of *Tg(Tp1:* mCherry)-positive cells. 79.8±2.7% of *Tg(Tp1:*mCherry)-positive cells were CFP^+ in the MTZ-treated regenerating livers, while 16.7±1.3% of *Tg(Tp1:*mCherry)-positive cells expressed CFP in the EtOH/MTZ-treated regenerating livers. Cells in 5 planes of confocal images from 5 individual larvae were counted. Asterisks indicate statistical significance: ****p*<0.001. All confocal images are single-plane images except A’, B’ and C’, which are projection images (n=15 larvae per condition in three experiments). Scale bar, 20μm. EtOH, ethanol; SD, standard deviation.

Supporting Fig. 4. Alcam is not expressed in a population of cells co-expressing hepatocyte-specific CFP and NRC-specific mCherry. (A-A’’’) In [*Tg(fabp10a:CFP-NTR)*^{gt1}*; Tg(Tp1:mCherry)*^{jh11}; *Tg(hand2:EGFP)*^{pd24}] larvae treated with DMSO at 5 dpf, a biliary epithelial cell marker, activated leukocyte cell adhesion molecule (Alcam), is expressed in all of NRCs (A’’, inset). Quiescent HSCs showed a star-shaped configuration (A’, inset). (B-B’’’) Hepatocytes were ablated by MTZ and allowed to regenerate for 50 hours. In the MTZ-treated regenerating livers, bright red NRCs remained CFP negative and Alcam positive (B’’, B’’’, insets, yellow arrowheads), while a population of cells co-expressing hepatocyte-specific CFP and NRC-specific

nuclear mCherry was Alcam negative (B’’, B’’’, insets, white arrows). The number of HSCs increased (B’). (C-C’’’) The larvae were pretreated with 1.5% EtOH from 2.5 to 3.5 dpf and then concurrently treated with MTZ from 3.5 to 4.5 dpf and allowed to regenerate for 50 hours. The Alcam negative NRCs co-expressing CFP and dim mCherry (C’’, C’’’, insets, white arrows) were distinguishable from the bright red NRCs that were negative for CFP and positive for Alcam (C’’, C’’’, insets, yellow arrowheads). HSCs increased in number and lost complex cytoplasmic processes (C’, inset). (D-D’’’) Larvae were treated with 1.5% EtOH from 2.5 to 4.5 dpf and allowed to grow for 50 hours. Moderate increase of the number of HSCs and the morphology change were observed (D’, inset). All of the NRCs were Alcam positive (D’’) with no cells co-expressing hepatocyte-specific CFP and NRC-specific nuclear mCherry (D’’’). All confocal images are single-plane images except A’, B’, C’ and D’, which are projection images (n=15 larvae per condition in three experiments). Scale bar, 20μm.

Supporting Fig. 5. The liver function restores and is maintained after near-complete destruction of hepatocytes. (A-D’) Fluorescent or bright-field images of DMSO- (A, A’), MTZ- (B, B’, C, C’) or EtOH/MTZ- (D, D’) treated regenerating larvae. The MTZ-treated regenerating larvae incubated with PED6 showed an accumulation of the processed PED6 in the gallbladder at 96 hpa (C, arrow) as seen in the DMSO-treated controls at 5 dpf (A, arrow), while no PED6 accumulation was observed at 0 hpa (B, arrow). No discernible morphological defects were detected in the MTZ-treated regenerating larvae at 96 hpa (C’) as in the DMSO-treated controls at 5 dpf (A’). EtOH/MTZ-treated regenerating larvae showed decreased efficiency of PED6 processing

(D, arrow) with morphological abnormalities (D’) at 96 hpa. (E-L) Confocal images of regenerating larvae or regenerated fish showed morphologically and functionally comparable hepatocytes and an intrahepatic biliary ductal network to that of the DMSO-treated controls. Alcam is expressed in NRCs of the MTZ-treated regenerating larvae and fish at 96 hpa (F) and at 1 months-post-ablation (mpa) (G), respectively, as in the DMSO-treated controls at 5 dpf (E). Expression of Abcb11, a bile transport pump located in the bile canaliculi of hepatocytes was restored in the MTZ-treated regenerating larvae and fish at 96 hpa (J) and at 1 mpa (K), respectively, as in the DMSO-treated controls at 5 dpf (I). EtOH/MTZ-treated regenerating larvae showed evident Alcam (H) and Abcb11 (L) expression with a slower efficiency of regeneration at 96 hpa. A-D’, fluorescent or bright-field images (n=15 larvae per condition in three experiments). E-L, confocal single-plane images (E, F, H, I, J and L, n=9 larvae per condition in three experiments; G and K, n=5 fish). Scale bars: A-D’, 100μm; E-L, 20μm. EtOH, ethanol.

Supporting Fig. 6. Heterogeneity of Notch signaling activity in the EtOH/MTZ-treated regenerating livers. (A-E) EtOH/MTZ-treated [*Tg(fabp10a:CFP-NTR)*^{gt1}*; Tg(Tp1:mCherry)*^{jh11}] larvae were collected at the indicated time points during liver regeneration. Yellow arrowheads indicate bright red NRCs with Alcam expression, while white arrows indicate dim red NRCs without Alcam expression including NRCs co-expressing hepatocyte-specific CFP. (A) NRCs marked by *Tg(Tp1:*mCherry) clustered together in close proximity at 0 days-post-ablation (dpa). (B) The number of mCherry-expressing NRCs slightly expanded at 1 dpa. (C) At 2 dpa, hepatocyte-specific CFP started to co-express in a few dimming mCherry-positive NRCs throughout the

regenerating livers (white arrows), while the bright red NRCs remained (yellow arrowheads). (D) At 3 dpa, dim red NRCs co-expressing CFP (white arrows) continued to increase in numbers. (E) CFP-positive NRCs became CFP only-positive cells with the loss of red (white arrows), persisting to increase in numbers at 4 dpa. The bright red NRCs remained as CFP-negative (yellow arrowheads). (F) Percentages (mean±SD) of dim red NRCs that contributed to newly formed CFP-positive hepatocytes in the first 4 days of regeneration. The percentage of dim red NRCs increased (0 dpa, 7.7±1.2%; 1 dpa, 12.9±2.0%; 2 dpa, 38.4±5.3%; 3 dpa, 80.4±7.4%; 4dpa, 82.9±4.2%) during the regeneration with all of the CFP-positive hepatocytes being derived from these cells (2 dpa, 16.1±3.5%; 3 dpa, 33.3±5.1%; 4 dpa, 82.9±4.2%). Cells in 5 planes of confocal images from 5 individual larvae were counted at each time point. All images are confocal single-plane images (n=15 larvae per each time point in three experiments). Scale bars, 20μm. EtOH, ethanol; SD, standard deviation.

Supporting Fig. 7. Heterogeneity of Notch signaling activity in the [*Tg(fabp10a:mCherry-NTR)*^{gt2}; *Tg(Tp1:EGFP)*^{um14}] regenerating larvae. (A) In the DMSO-treated control larvae, expression of *Tg(fabp10a:*mCherry-NTR) marks hepatocytes, while that of *Tg(Tp1:*EGFP) marks the cell bodies and cytoplasmic extensions of NRCs. (B-E) MTZ-treated larvae were collected at the indicated time points during liver regeneration. (B) NRCs marked by *Tg(Tp1:*EGFP) clustered together in close proximity at 0 hpa. (C) At 13-15 hpa, hepatocyte-specific mCherry started to co-express in a few EGFP-positive NRCs (inset, white arrows). (D) At 25 hpa, NRCs were clearly segregated into two heterogeneous populations, dim green NRCs

co-expressing mCherry (inset, white arrows) and bright green NRCs without mCherry markers (inset, yellow arrowhead). (E) mCherry-positive NRCs became mCherry only-positive cells with the loss of green (white arrows), continuing to increase in numbers at 50 hpa. Bright green NRCs remained as mCherry-negative. (F-J) EtOH/MTZ-treated larvae were collected at the indicated time points during liver regeneration. NRCs marked by *Tg(Tp1:*EGFP) clustered together in close proximity at 0 dpa (F) and moderately increased in number at 1 dpa (G). mCherry and EGFP co-expressing NRCs started to appear at 2 dpa (H, inset, white arrows) and continued to increase in number at 3 dpa (I, inset, white arrows) and 4 dpa (J, white arrows). All images are confocal single-plane images (A-E, n=30 larvae per each time point in three experiments; F-J, n=15 larvae per each time point in three experiments). Scale bar, 20μm. EtOH, ethanol.

Supporting Fig. 8. An endothelial cell- or stellate cell-to-hepatocyte conversion is a rare event in the regenerating livers. [*Tg(fabp10a:mCherry-NTR)*^{gt2};*Tg(kdrl:EGFP)*^{s843}] (A) and [*Tg(fabp10a:mCherry-NTR)*^{gt2}; *Tg(hand2:EGFP)*^{pd24}] (C) livers treated with DMSO. Coexpression of *kdrl*-EGFP and *fabp10a*-mCherry (B, inset) or *hand2*-EGFP and *fabp10a*-mCherry (D, inset) was seldom observed in the regenerating livers. All images are confocal single-plane images (n=30 larvae per condition in three experiments). Scale bar, 20μm.

Supporting Fig. 9. A genetic inducible fate mapping suggests that NRCs encompass a population of cells with potential to regenerate as hepatocytes. (A-B') Incubation of

4-hydroxytamoxifen (4-OHT) prior to MTZ treatement (24-48 hpf). In the MTZ-treated regenerating livers, a subset of mCherry-expressing NRCs co-expressed hepatocyte-specific CFP at 35 hpa (B, B', white arrows) in the presence of mCherry-expressing NRCs that were negative for CFP and positive for Alcam (B, B', yellow arrowheads). In the control livers without MTZ treatment, mCherry NRCs were only detected in the Alcam-positive biliary epithelial cells but not in the hepatocytes (A, yellow arrowheads). (C-D') Incubation of 4-OHT after hepatocyte ablation (from 0 to 24 hpa, equivalent to 120-144 hpf) led to the occurrence of CFP and mCherry co-expressing NRCs at 35 hpa in the MTZ-treated regenerating livers (D, D', white arrows) in the presence of mCherry-expressing NRCs that were negative for CFP and positive for Alcam (D, D', yellow arrowheads). In the control livers without MTZ treatment, mCherry NRCs were only observed in the Alcam-positive biliary epithelial cells but not in the hepatocytes (C, yellow arrowheads). (E, F) Larvae treated with 4-OHT between 24-48 hpf followed by MTZ ablation were allowed to grow until 1 months-post-ablation (mpa). mCherry-expressing hepatocytes, which were derived from a subset of NRCs, reconstituted the liver (white arrows). Expression of Alcam (E) and Abcb11 (F) showed restoration of the morphologically and functionally intact hepatocytes and the intrahepatic biliary ductal network in these regenerated fish. All images are confocal single-plane images (A-B', n=30 larvae per condition in three experiments; C-D', n=15 larvae per condition in three experiments; E-F, n=5 fish). Scale bars, 20μm.

Supporting Fig. 10. Distinct levels of Notch signaling are essential for the differentiation of the HPCs into hepatocytes in the EtOH/MTZ-treated regenerating livers. (A-E)

EtOH/MTZ-treated [*Tg(fabp10a:CFP-NTR)*^{gt1}*; Tg(Tp:H2BmCherry)*^{s939}*; Tg(Tp1:VenusPEST)*^{s940}] larvae were collected at the indicated time points during liver regeneration. (A) At 0 hpa, *Tg(Tp1:*H2BmCherry)-positive NRCs were segregated into *Tg(Tp1:*VenusPEST*)*$^{-}$/Alcam^{-} (white arrowhead), *Tg(Tp1:*VenusPEST*)*^{low}/Alcam^{+} (red arrowheads), and *Tg(Tp1:*VenusPEST*)*^{high} /Alcam^{+} (yellow arrowheads) group based on the intensity of Venus and Alcam expression. (B-C') The proportion of *Tg(Tp1:*VenusPEST*)*$^{-}$/Alcam^{-} cells (white arrowheads) started increasing in the regenerating livers with a decrease in *Tg(Tp1:*VenusPEST*)*^{low}/Alcam^{+} cells (red arrowheads) at 1-2 dpa. At 2 dpa (C, C'), converting CFP-positive NRCs (white arrows) were observed in *Tg(Tp1:*VenusPEST*)*$^{-}$/Alcam^{-} cells. (D) The population of *Tg(Tp1:*VenusPEST*)*$^{-}$/Alcam^{-}/CFP^{+} cells (white arrows) expanded at 3 dpa. (E) All the converting CFP-positive NRCs (white arrows) were *Tg(Tp1:*VenusPEST*)*$^{-}$/Alcam^{-} cells with near absence of *Tg(Tp1:*VenusPEST*)*^{low}/Alcam^{+} cells at 4 dpa. Therefore, the *Tg(Tp1:*VenusPEST*)*^{low} /Alcam^{+} (red arrowheads) and *Tg(Tp1:*VenusPEST*)*$^{-}$/Alcam^{-} cells (white arrowheads) experiencing different degrees of Notch downregulation at early stages of liver regeneration may equate to the transitioning HPCs. (F) Percentage (mean ±SD) of *Tg(Tp1:*VenusPEST*)*$^{-}$/Alcam^{-} (0 dpa, 16.0±2.3%; 1 dpa, 32.2±4.2%; 2 dpa, 50.7±9.5%; 3 dpa, 84.8±8.6%; 4 dpa, 91.5±11.2%), *Tg(Tp1:*VenusPEST*)*^{low}/Alcam^{+} (0 dpa, 64.0±13.2%; 1 dpa, 53.0±12.5%; 2 dpa, 39.6±9.8%; 3 dpa, 6.4±1.3%), *Tg(Tp1:*VenusPEST*)*^{high} /Alcam^{+} (0 dpa, 20.0±4.3%; 1 dpa, 14.8±2.3%; 2 dpa, 9.7±1.2%; 3 dpa, 8.8±2.0%; 4 dpa, 8.5±1.5%), and *Tg(Tp1:*VenusPEST*)*$^{-}$/Alcam^{-}/CFP^{+} cells (2 dpa, 16.1±2.4%; 3 dpa, 35.0±3.3%; 4 dpa, 91.5±11.2%) during hepatocyte regeneration. Cells in 5 planes of confocal images from 5 individual larvae were counted at each time point.

All images are confocal single-plane images except B' and C', which are projection images (n=15 larvae per each time point in three experiments). Scale bars, 20μm.

Supporting Fig. 11. Identification of a population of cells experiencing Notch downregulation during hepatocyte ablation. (A, A') By comparing the expression dynamics of VenusPEST and mCherry, two distinct populations of mCherry cells, dim and bright red, were detected at 0 hpa, further diverging *Tg(Tp1:* mCherry)-positive NRCs into 4 groups at 0 hpa: *Tg(Tp1:*mCherry*)*^{dim}/*Tg(Tp1:*VenusPEST*)*$^{-}$/Alcam^{-} (white arrowhead), *Tg(Tp1:*mCherry*)*^{bright}/*Tg(Tp1:*VenusPEST*)*$^{-}$/Alcam^{-} (red arrow), *Tg(Tp1:*mCherry*)*^{bright}/*Tg(Tp1:*VenusPEST*)*^{low}/Alcam^{+} (red arrowheads), and *Tg(Tp1:*mCherry*)*^{bright}/*Tg(Tp1:*VenusPEST*)*^{high}/Alcam^{+} (yellow arrowheads). (B-C') The proportion of *Tg(Tp1:*VenusPEST*)*$^{-}$/Alcam^{-} cells (white arrowheads and red arrows) started increasing in the MTZ-treated regenerating livers with the decrease of *Tg(Tp1:*mCherry*)*^{bright}/*Tg(Tp1:*VenusPEST*)*^{low}/Alcam^{+} cells (red arrowheads) at 5-10 hpa. (D, E) At 15 hpa, *Tg(Tp1:*mCherry*)*^{dim}/*Tg(Tp1:*VenusPEST*)*$^{-}$/Alcam^{-}/CFP^{+} cells (white arrows) emerged. The dim red mCherry cells were only present in the *Tg(Tp1:*VenusPEST*)*$^{-}$/Alcam^{-} population, in which all CFP-positive hepatocytes were derived from, with significant increase in their percentage between 15 and 25 hpa. (F) At 50 hpa, only *Tg(Tp1:*mCherry*)*^{bright}/*Tg(Tp1:*VenusPEST*)*^{high}/Alcam^{+} (yellow arrowheads) and *Tg(Tp1:*mCherry*)*^{dim}/*Tg(Tp1:*VenusPEST*)*$^{-}$/Alcam^{-}/CFP^{+} cells (white arrows) can be observed. (G) Percentage (mean±SD) of *Tg(Tp1:*mCherry*)*^{dim}/*Tg(Tp1:*VenusPEST*)*$^{-}$/Alcam^{-} (0 hpa, 7.1±1.9%; 5 hpa, 12.2±2.6%; 10 hpa, 18.0±3.1%; 15 hpa, 25.0±4.9%; 25 hpa, 63.5±6.2%; 50 hpa, 87.5±0.7%),

*Tg(Tp1:*mCherry*)*^{bright}/*Tg(Tp1:*VenusPEST*)*$^{-}$/Alcam^{-} (0 hpa, 7.9±0.4%; 5 hpa, 19.8±3.0%; 10 hpa, 28.6±3.8%; 15 hpa, 38.2±7.2%; 25 hpa, 18.3±2.1%), *Tg(Tp1:*mCherry*)*^{bright}/*Tg(Tp1:*VenusPEST*)*^{low}/Alcam^{+} (0 hpa, 59.9±4.3%; 5 hpa, 48.1±3.7%; 10 hpa, 35.4±0.8%; 15 hpa, 22.3±3.1%; 25 hpa, 5.2±1.2%), *Tg(Tp1:*mCherry*)*^{bright}/*Tg(Tp1:*VenusPEST*)*^{high}/Alcam^{+} (0 hpa, 25.1±6.6%; 5 hpa, 19.9±2.2%; 10 hpa, 18.0±1.8%; 15 hpa, 14.5±4.4%; 25 hpa, 13.0±3.6%; 50 hpa, 12.5±0.7%), and *Tg(Tp1:*mCherry*)*^{dim}/*Tg(Tp1:*VenusPEST*)*$^{-}$/Alcam^{-}/CFP^{+} cells (15 hpa, 16.7±0.8%; 25 hpa, 42.3±2.6%; 50 hpa, 87.5±0.7%) during hepatocyte regeneration. Cells in 5 planes of confocal images from 5 individual larvae were counted at each time point. All images are confocal single-plane images except A', B', and C', which are projection images (n=15 larvae per each time point in three experiments). Scale bars, 20μm.

Supporting Fig. 12. The level of Notch signaling is essential for hepatocyte differentiation. (A-F) Inhibition of Notch signaling by LY411575 promoted hepatocyte differentiation. MTZ- (A-B') or EtOH/MTZ- (D-E') treated livers in [*Tg(fabp10a:CFP-NTR)*^{gt1}*; Tg(Tp1:H2BmCherry)*^{s939}; *Tg*(*Tp1:VenusPEST*)^{s940}] larvae were treated with DMSO (A, A', D, D') or 50μM Notch inhibitor LY411575 (B, B', E, E'). LY411575 treatment significantly augmented hepatocyte regeneration (B, B', E, E'). (C, F) Percentage (mean±SD) of CFP-positive cells in the population of *Tg(Tp1:* H2BmCherry)-positive cells. 17.8±2.3% of *Tg(Tp1:* H2BmCherry)-positive cells were CFP^{+} in the DMSO treatment, while LY411575 treatment significantly increased the proportion of CFP^{+} cells to 33.2±2.8% in the MTZ-treated regenerating livers (C). In the

EtOH/MTZ-treated regenerating livers, 15.9±3.1% of *Tg(Tp1:* H2BmCherry)-positive cells were CFP^+ in the DMSO treatment, while LY411575 treatment significantly increased the proportion of CFP^+ cells to 28.4±2.4% (F). ***p<0.001. (G-I) Overexpression of Notch1a intracellular domain attenuated hepatocyte differentiation. MTZ-treated livers in [*Tg(fabp10a:CFP-NTR)*^{gt1}*; Tg(Tp1:mCherry)*^{jh11}*; Tg(hsp:GAL4)*^{kca4}*; Tg(UAS:myc-Notch1a-Intra*)^{kca3}] larvae were heat shocked to overexpress Notch1a intracellular domain. Upregulation of *Tg(Tp1:*mCherry) showed evidence of high Notch signal induction after heat shock in the NICD-positive livers, outlined with white dashed lines (H, H'). (I) Percentage (mean±SD) of CFP^+ cells in the population of *Tg(Tp1:* mCherry)-positive cells. 13.4±2.4% of *Tg(Tp1:*mCherry)-positive cells were CFP-positive in the MTZ-treated control larvae without heat shock, whereas overexpression of Notch1 intracellular domain significantly decreased the proportion of CFP^+ cells to 4.2±0.8%. ***p<0.001. Cells in 5 planes of confocal images from 5 individual larvae were counted. All images are confocal projection images (A-B' and G-H', n=30 larvae per condition in three experiments; D-E', n=15 larvae per condition in three experiments). Scale bars, 20μm. EtOH, ethanol; SD, standard deviation.

Supporting Fig. 13. Wnt agonist has no detrimental effect on biliary secretion. (A-B') Fluorescent or bright-field images of MTZ/CHIR99021- (A, A') or EtOH/MTZ/CHIR99021- (B, B') treated regenerating larvae. The MTZ/CHIR99021-treated regenerating larvae incubated with PED6 showed an accumulation of the processed PED6 in the gallbladder at 96 hpa (A, arrow). No discernible morphological defects were detected in the MTZ/CHIR99021-treated

regenerating larvae (A'). EtOH/MTZ/CHIR99021-treated regenerating larvae showed decreased efficiency of PED6 processing (B, arrow) with morphological abnormalities (B'). Alcam is expressed in NRCs of the MTZ/CHIR99021-treated regenerating larvae at 96 hpa (C). Expression of Abcb11, a bile transport pump located in the bile canaliculi of hepatocytes was restored in the MTZ/CHIR99021-treated regenerating larvae at 96 hpa (E). EtOH/MTZ/CHIR99021-treated regenerating larvae showed evident Alcam (D) and Abcb11 (F) expression with a slower efficiency of regeneration at 96 hpa. A-B', fluorescent or bright-field images (n=15 larvae per condition in three experiments). C-F, confocal single-plane images (n=9 larvae per condition in three experiments). Scale bars: A-B', 100μm; C-F, 20μm.

Supporting Fig. 14. The Wnt signaling is essential for hepatocyte regeneration. Compared with the MTZ-treated controls without heat shock (A), overexpression of Wnt pathway ligand Wnt8a accelerated hepatocyte regeneration (B). (C) Percentage (mean±SD) of CFP^+ cells in the population of *Tg(Tp1:*mCherry)-positive cells. 16.5±1.9% of *Tg(Tp1:*mCherry)-positive cells were CFP^+ in the control larvae, whereas overexpression of Wnt8a significantly increased the proportion of CFP^+ cells to 34.5±3.4%. Compared with the MTZ-treated controls without heat shock (D), overexpression of Wnt pathway antagonist Axin1 hindered hepatocyte regeneration (E). (F) Percentage (mean±SD) of CFP^+ cells in the population of *Tg(Tp1:*mCherry)-positive cells. 14.8±2.6% of *Tg(Tp1:*mCherry)-positive cells were CFP^+ in the control larvae, whereas overexpression of Axin1 significantly decreased the proportion of CFP^+ cells to 8.6±1.9%. Cells in 5 planes of confocal images from 5 individual larvae were counted. Asterisks indicate

statistical significance: ***p<0.001. All images are confocal projection images (n=30 larvae per condition in three experiments). Scale bar, 20μm. EtOH, ethanol; SD, standard deviation.

Supporting References

1. Westerfield M. The zebrafish book. A guide for the laboratory use of zebrafish (Danio rerio). 4th ed., Univ. of Oregon Press, Eugene 2000.

2. Farooq M, Sulochana KN, Pan X, To J, Sheng D, Gong Z, et al. Histone deacetylase 3 (hdac3) is specifically required for liver development in zebrafish. Dev Biol 2008;317:336-353.

3. Her GM, Chiang CC, Chen WY, Wu JL. In vivo studies of liver-type fatty acid binding protein (L-FABP) gene expression in liver of transgenic zebrafish (Danio rerio). FEBS Lett 2003;538:125-133.

4. Parsons MJ, Pisharath H, Yusuff S, Moore JC, Siekmann AF, Lawson N, et al. Notch-responsive cells initiate the secondary transition in larval zebrafish pancreas. Mech Dev 2009;126:898-912.

5. Beis D, Bartman T, Jin SW, Scott IC, D'Amico LA, Ober EA, et al. Genetic and cellular analyses of zebrafish atrioventricular cushion and valve development. Development 2005;132:4193-4204.

6. Yin C, Kikuchi K, Hochgreb T, Poss KD, Stainier DY. Hand2 regulates extracellular matrix remodeling essential for gut-looping morphogenesis in zebrafish. Dev Cell 2010;18:973-984.

7. Wang Y, Rovira M, Yusuff S, Parsons MJ. Genetic inducible fate mapping in larval zebrafish reveals origins of adult insulin-producing beta-cells. Development 2011;138:609-617.

8. Ninov N, Borius M, Stainier DY. Different levels of Notch signaling regulate quiescence, renewal and differentiation in pancreatic endocrine progenitors. Development 2012;139:1557-1567.

9. Scheer N, Groth A, Hans S, Campos-Ortega JA. An instructive function for Notch in promoting gliogenesis in the zebrafish retina. Development 2001;128:1099-1107.

10. Scheer N, Campos-Ortega JA. Use of the Gal4-UAS technique for targeted gene expression in the zebrafish. Mech Dev 1999;80:153-158.

11. Weidinger G, Thorpe CJ, Wuennenberg-Stapleton K, Ngai J, Moon RT. The Sp1-related transcription factors sp5 and sp5-like act downstream of Wnt/beta-catenin signaling in mesoderm and neuroectoderm patterning. Curr Biol 2005;15:489-500.

12. Kagermeier-Schenk B, Wehner D, Ozhan-Kizil G, Yamamoto H, Li J, Kirchner K, et al. Waif1/5T4 inhibits Wnt/beta-catenin signaling and activates noncanonical Wnt pathways by modifying LRP6 subcellular localization. Dev Cell 2011;21:1129-1143.

13. Curado S, Anderson RM, Jungblut B, Mumm J, Schroeter E, Stainier DY. Conditional targeted cell ablation in zebrafish: a new tool for regeneration studies. Dev Dyn 2007;236:1025-1035.

14. Grabher C, Joly JS, Wittbrodt J. Highly efficient zebrafish transgenesis mediated by the meganuclease I-SceI. Methods Cell Biol 2004;77:381-401.

15. Farber SA, Pack M, Ho SY, Johnson ID, Wagner DS, Dosch R, et al. Genetic analysis of digestive physiology using fluorescent phospholipid reporters. Science 2001;292:1385-1388.

16. Untergasser A, Cutcutache I, Koressaar T, Ye J, Faircloth BC, Remm M, et al. Primer3--new capabilities and interfaces. Nucleic Acids Res 2012;40:e115.

17. Schmittgen TD, Livak KJ. Analyzing real-time PCR data by the comparative C(T) method. Nat Protoc 2008;3:1101-1108.

HEP-14-0077

Supporting Table 1. Effect of stem cell signaling compounds on liver regeneration

Compound	Target gene	Target signaling pathway (function)	Effect on liver regeneration
DAPT (GSI-IX)	γ-secretase	Notch (inhibitor)	Enhance
Semagacestat (LY450139)	γ-secretase	Notch (inhibitor)	Enhance
YO-01027	γ-secretase	Notch (inhibitor)	Enhance
LY411575	γ-secretase	Notch (inhibitor)	Enhance
TWS119	Glycogen synthase kinase-3	Wnt (activator)	Enhance
Indirubin	Glycogen synthase kinase-3	Wnt (activator)	Enhance
SB 415286	Glycogen synthase kinase-3	Wnt (activator)	Enhance
CHIR-99021 (CT99021) HCl	Glycogen synthase kinase-3	Wnt (activator)	Enhance
XAV-939	Tankyrase	Wnt (inhibitor)	Inhibit

HEP-14-0077

Supporting Fig.1

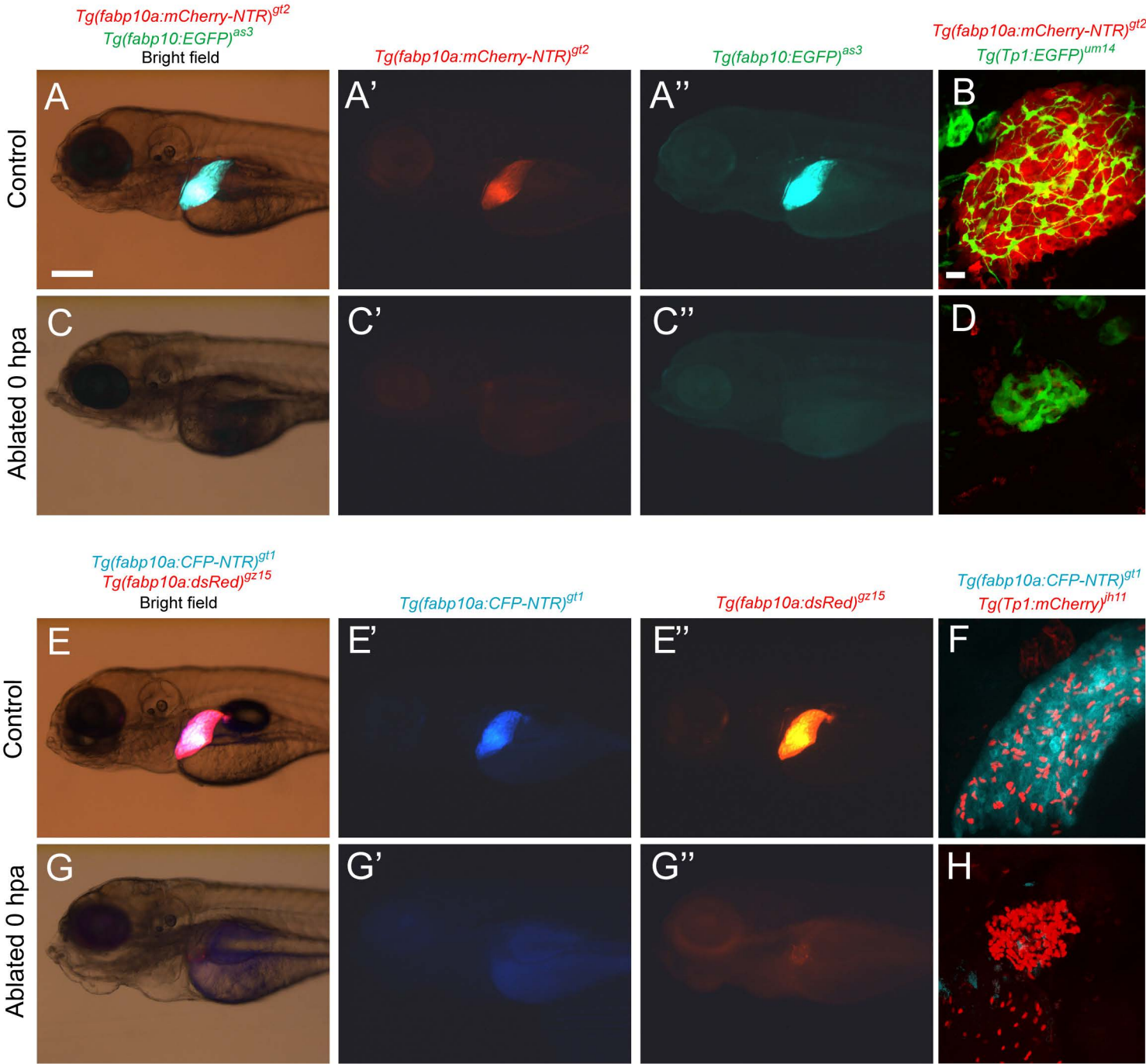

HEP-14-0077
Supporting Fig.2

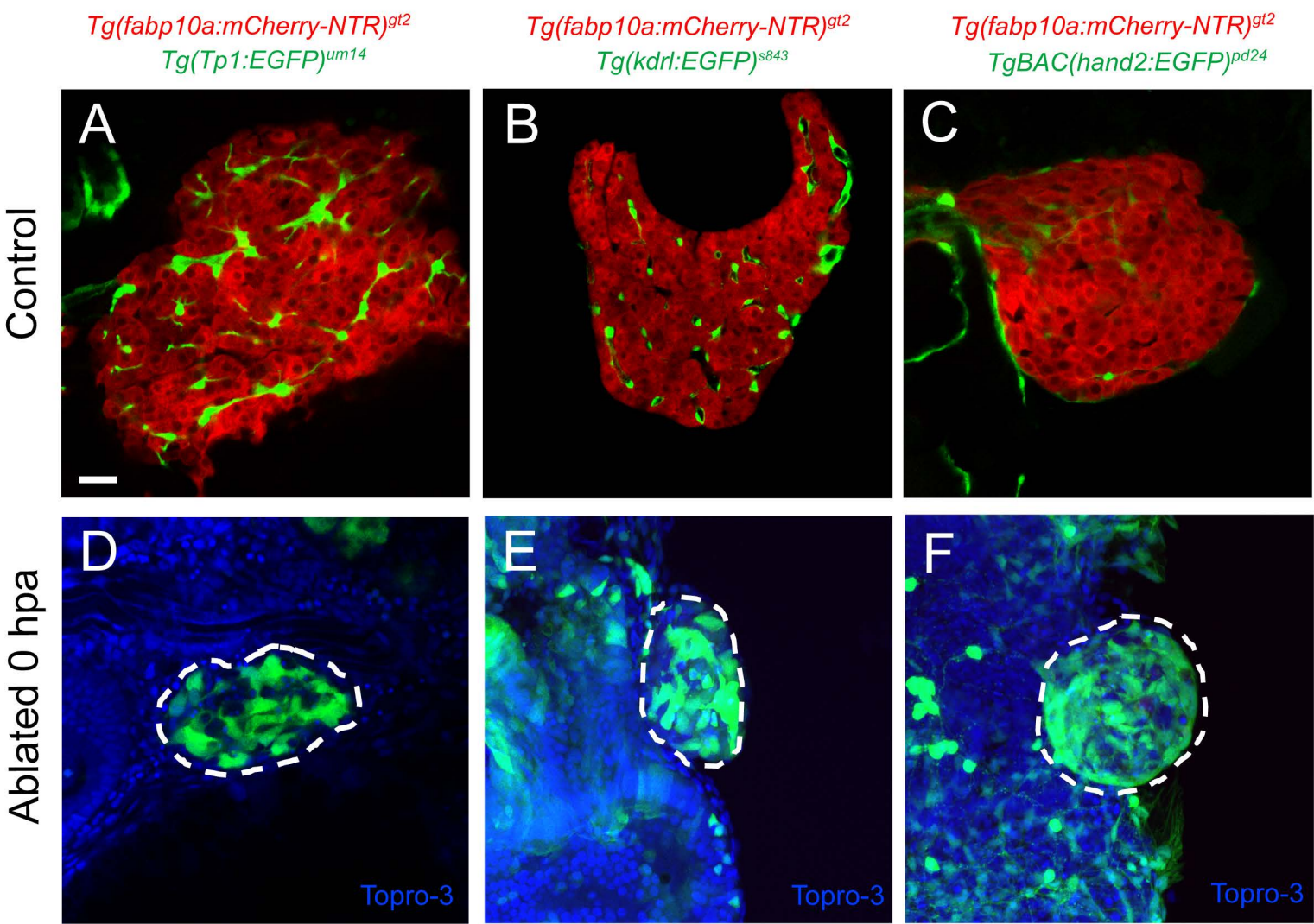

HEP-14-0077

Supporting Fig.3

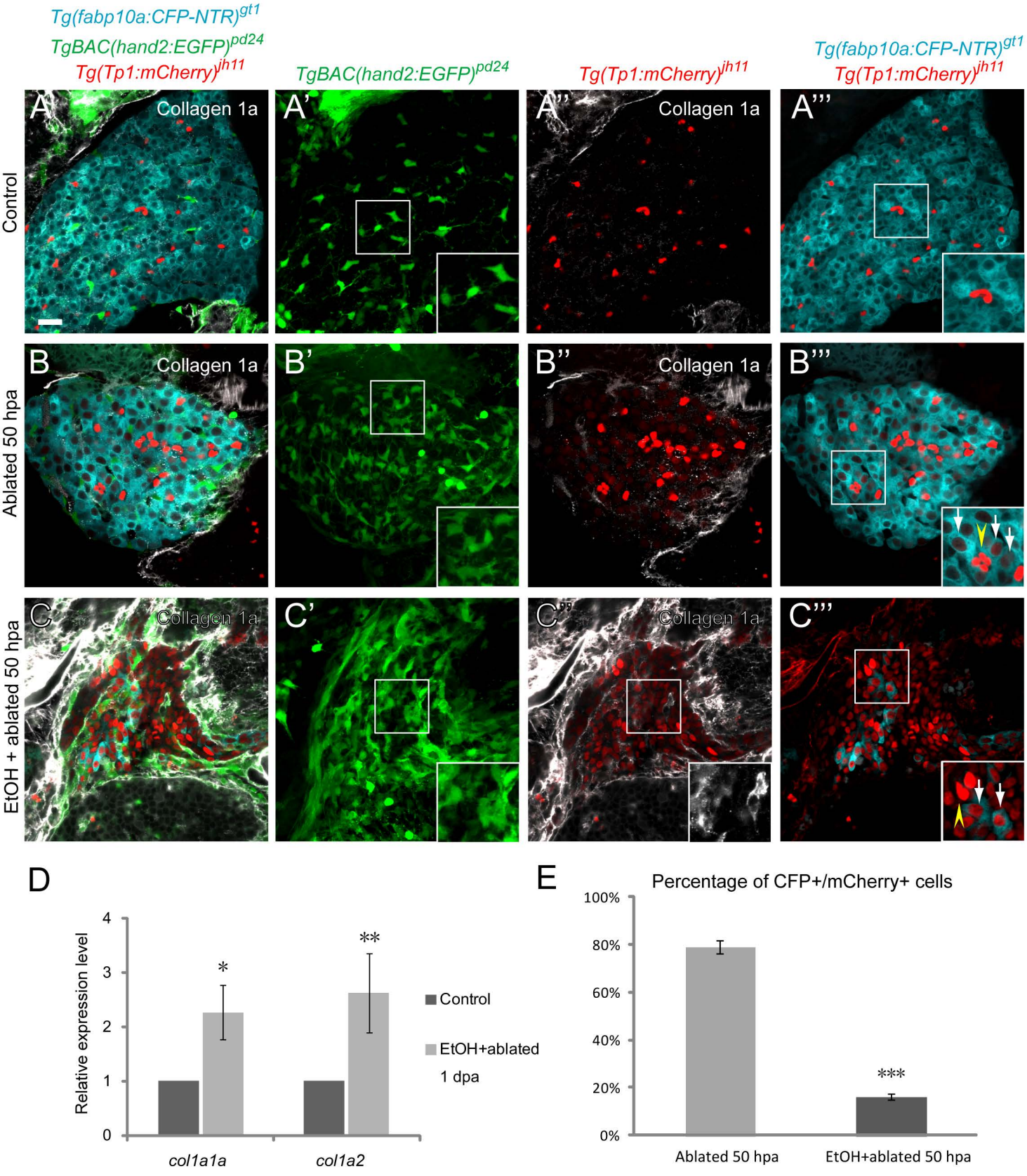

HEP-14-0077
Supporting Fig. 4

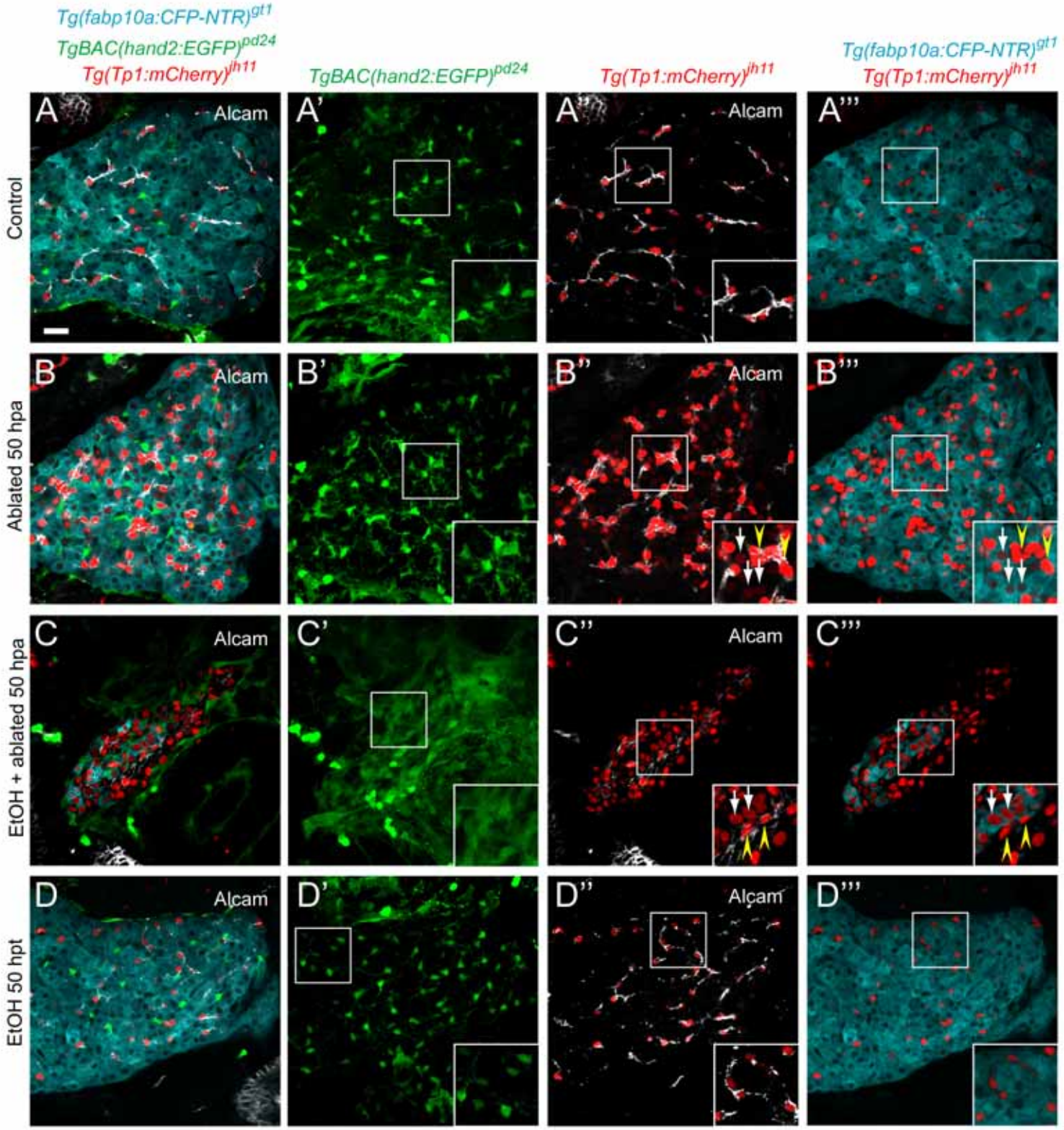

HEP-14-0077
Supporting Fig. 5

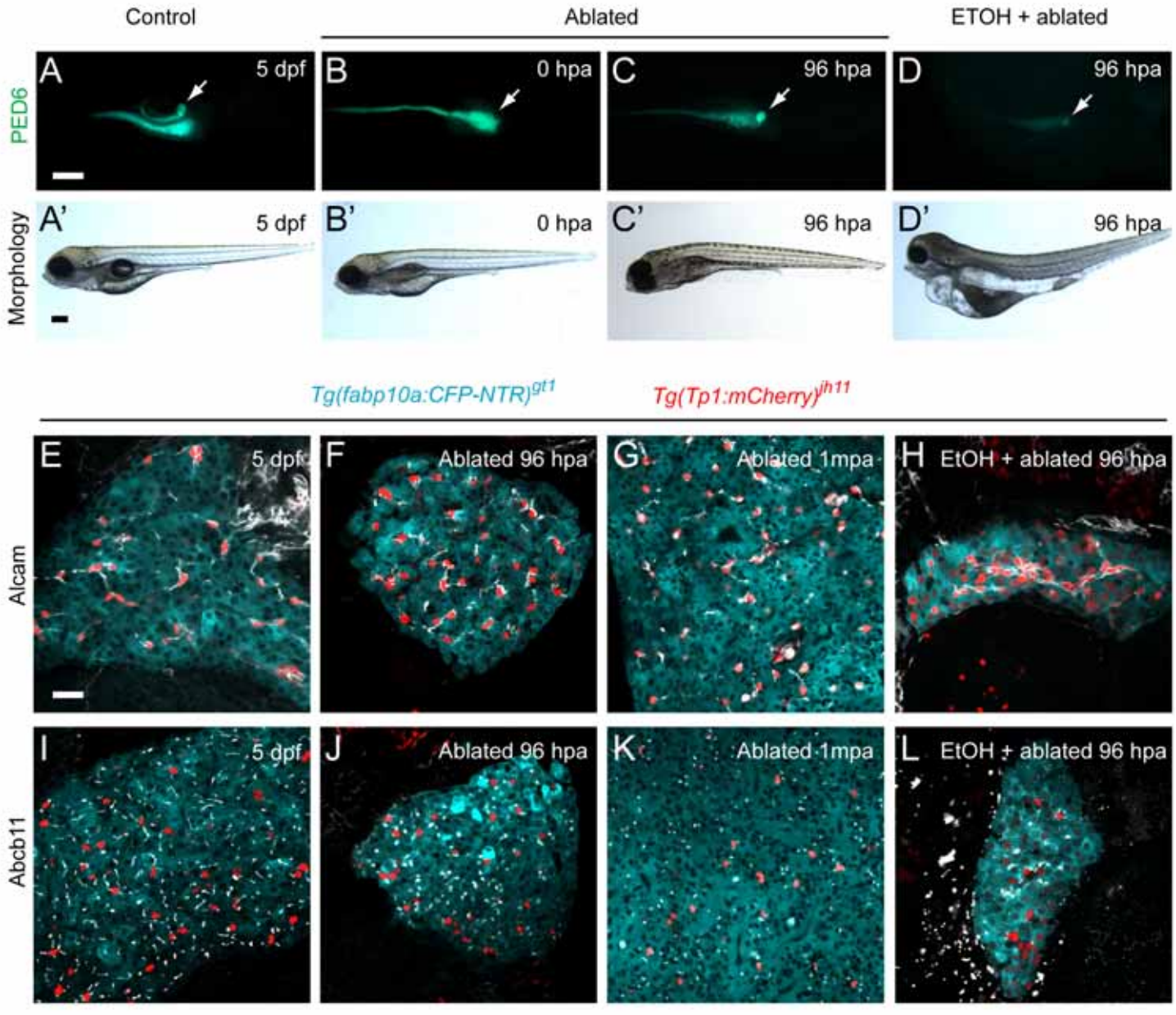

HEP-14-0077
Supporting Fig. 6

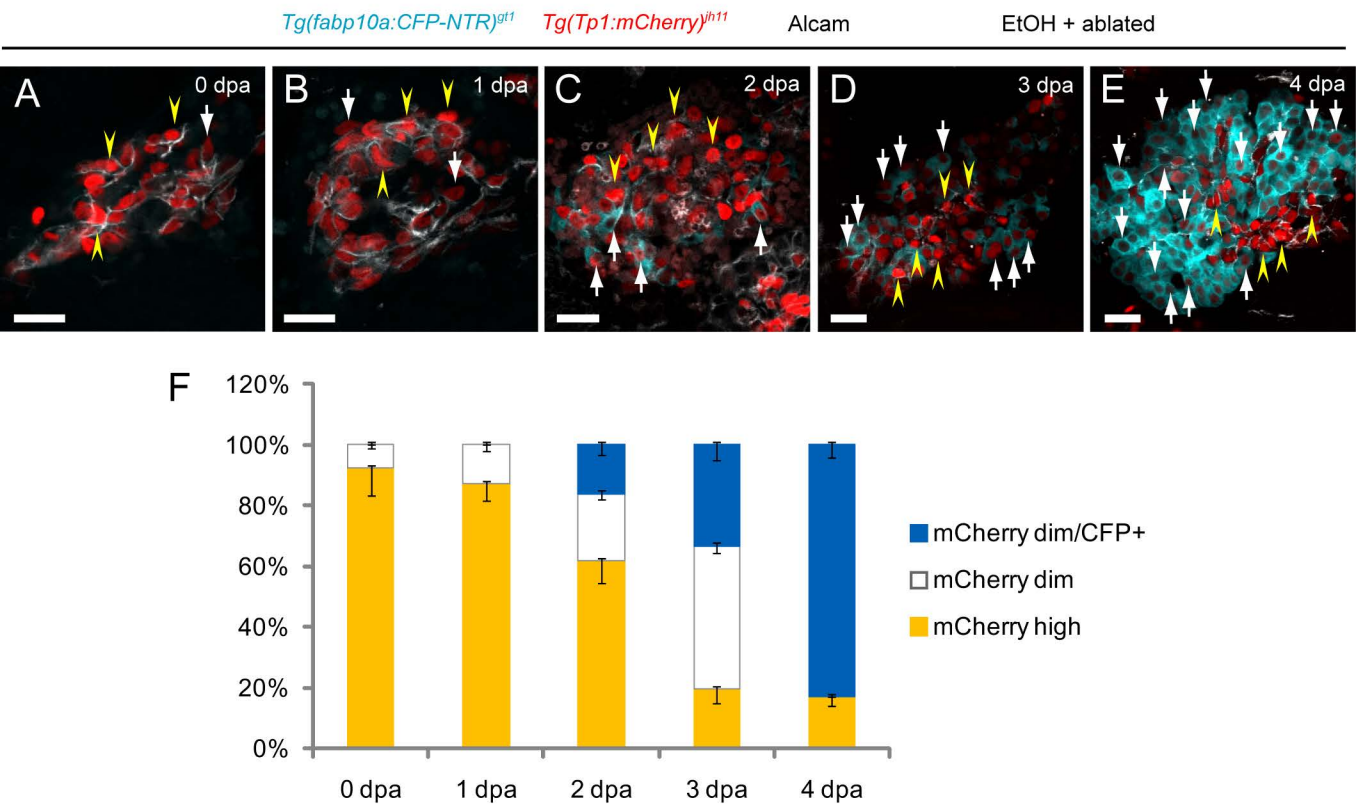

HEP-14-0077
Supporting Fig. 7

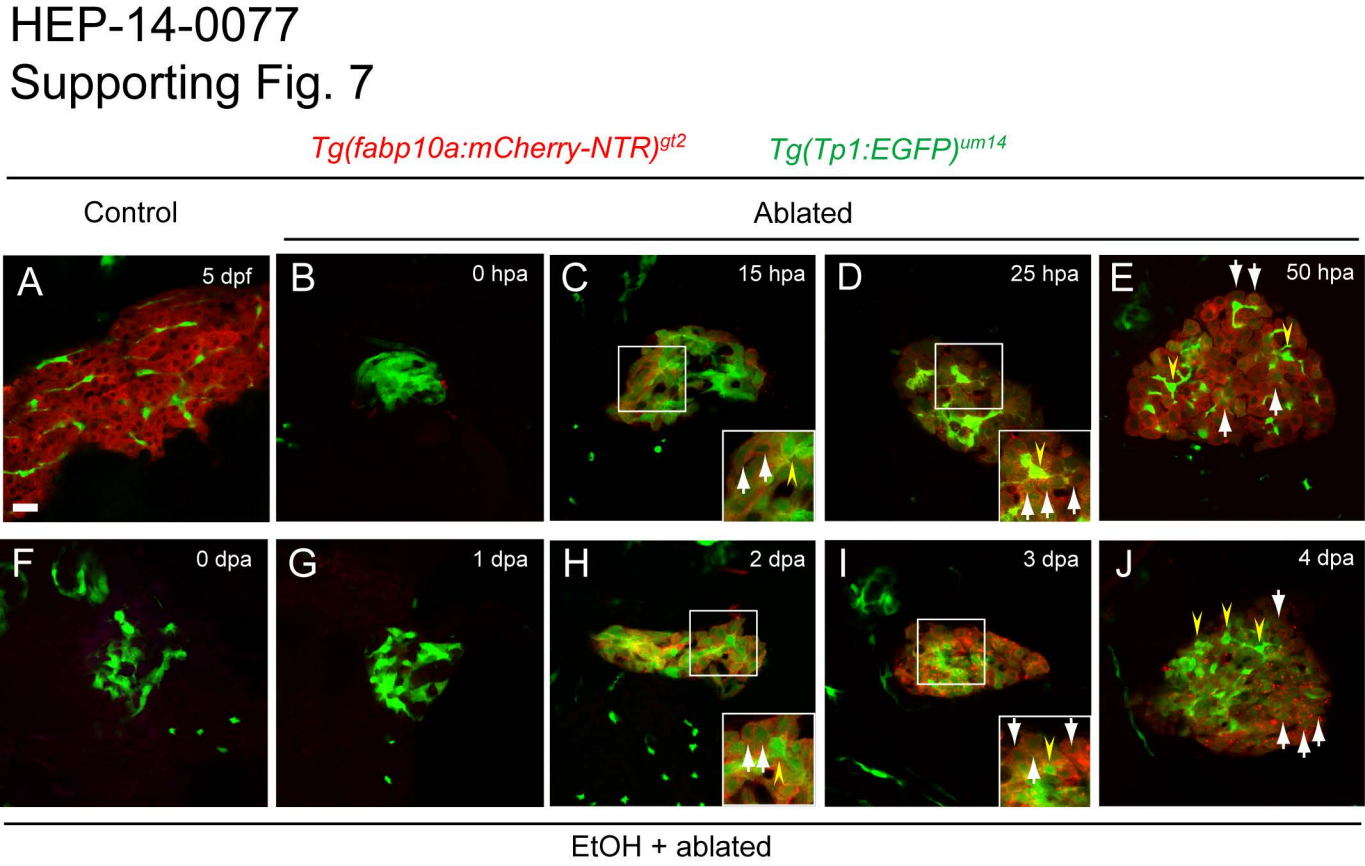

HEP-14-0077
Supporting Fig. 8

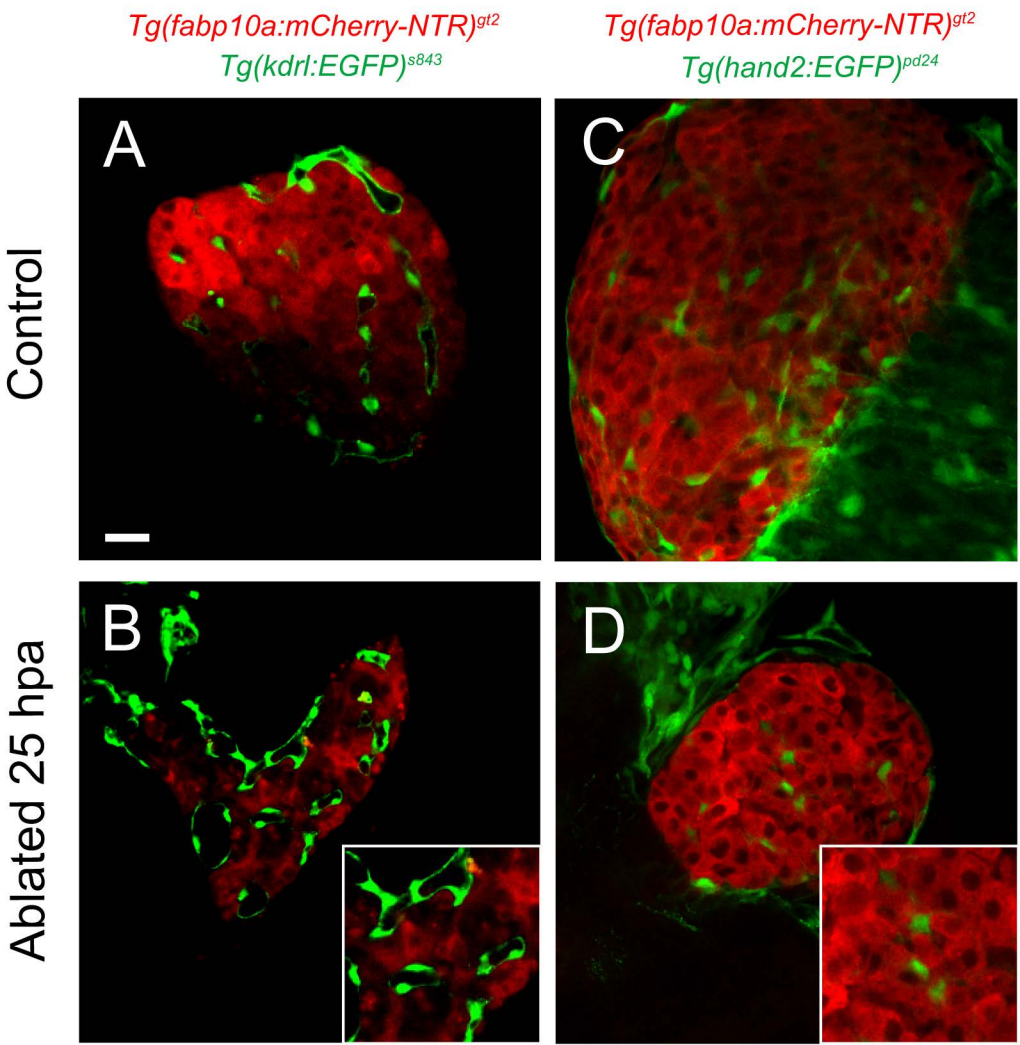

HEP-14-0077
Supporting Fig. 9

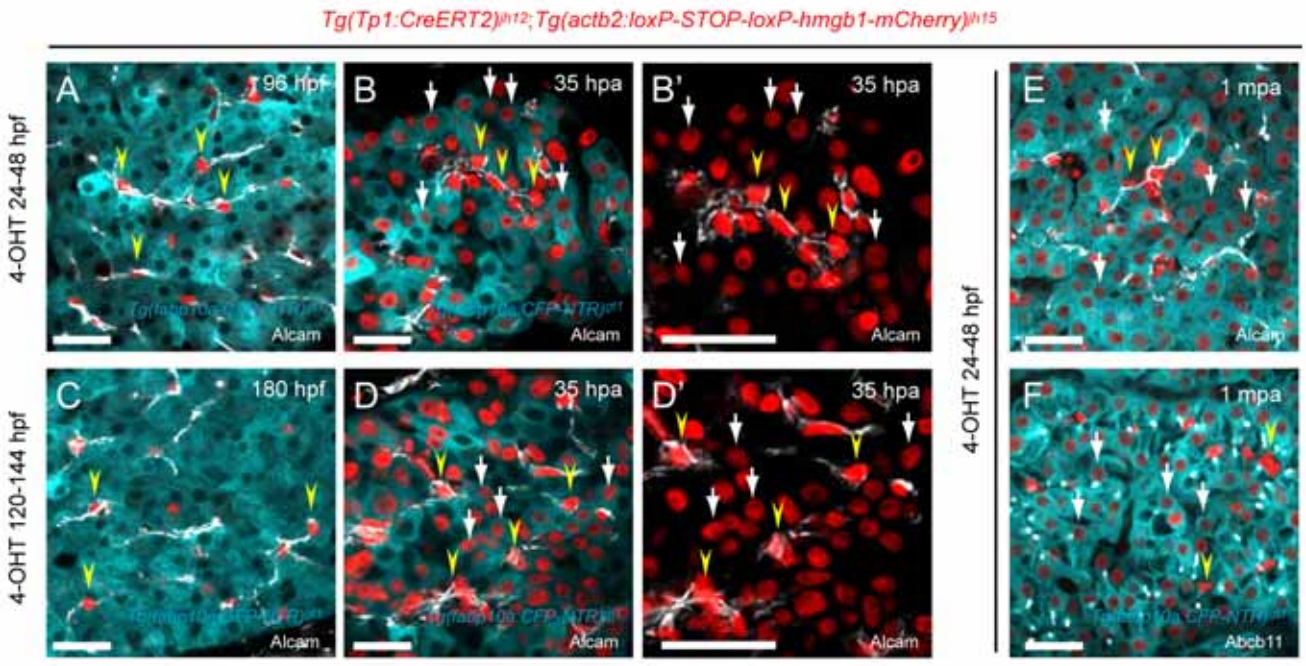

HEP-14-0077
Supporting Fig. 10

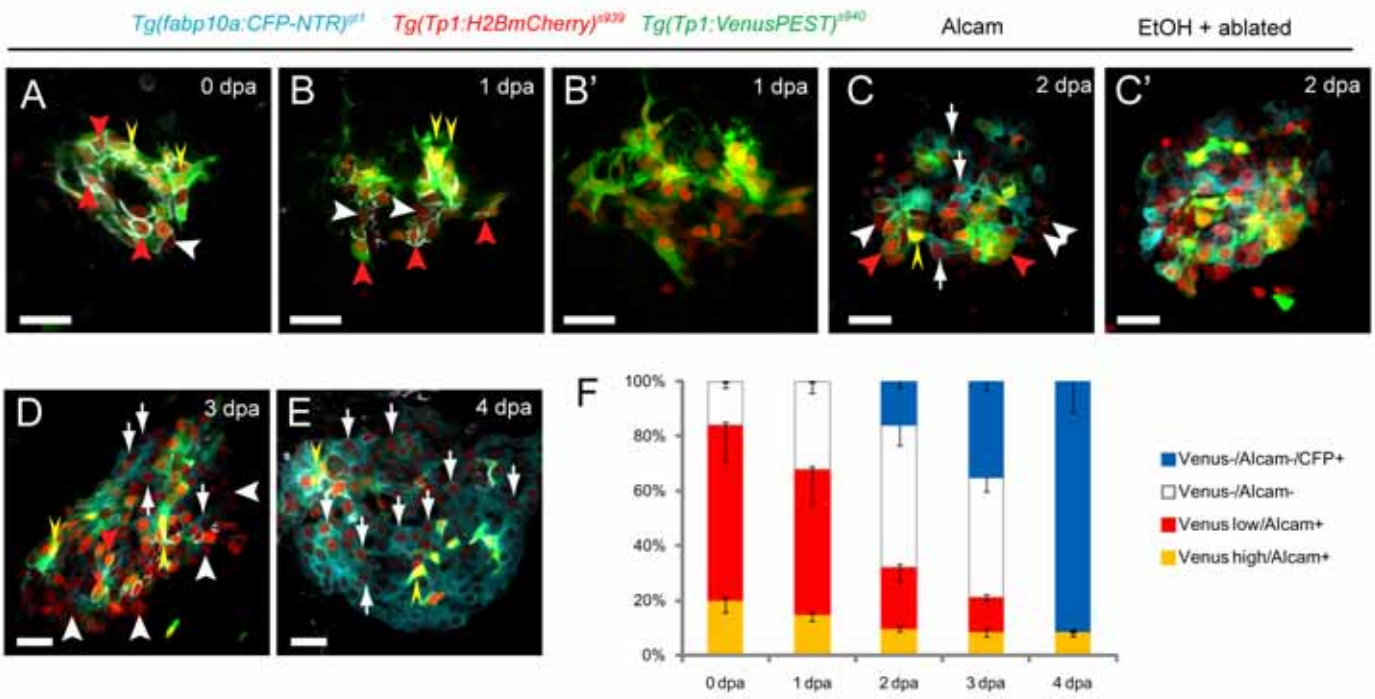

HEP-14-0077

Supporting Fig. 11

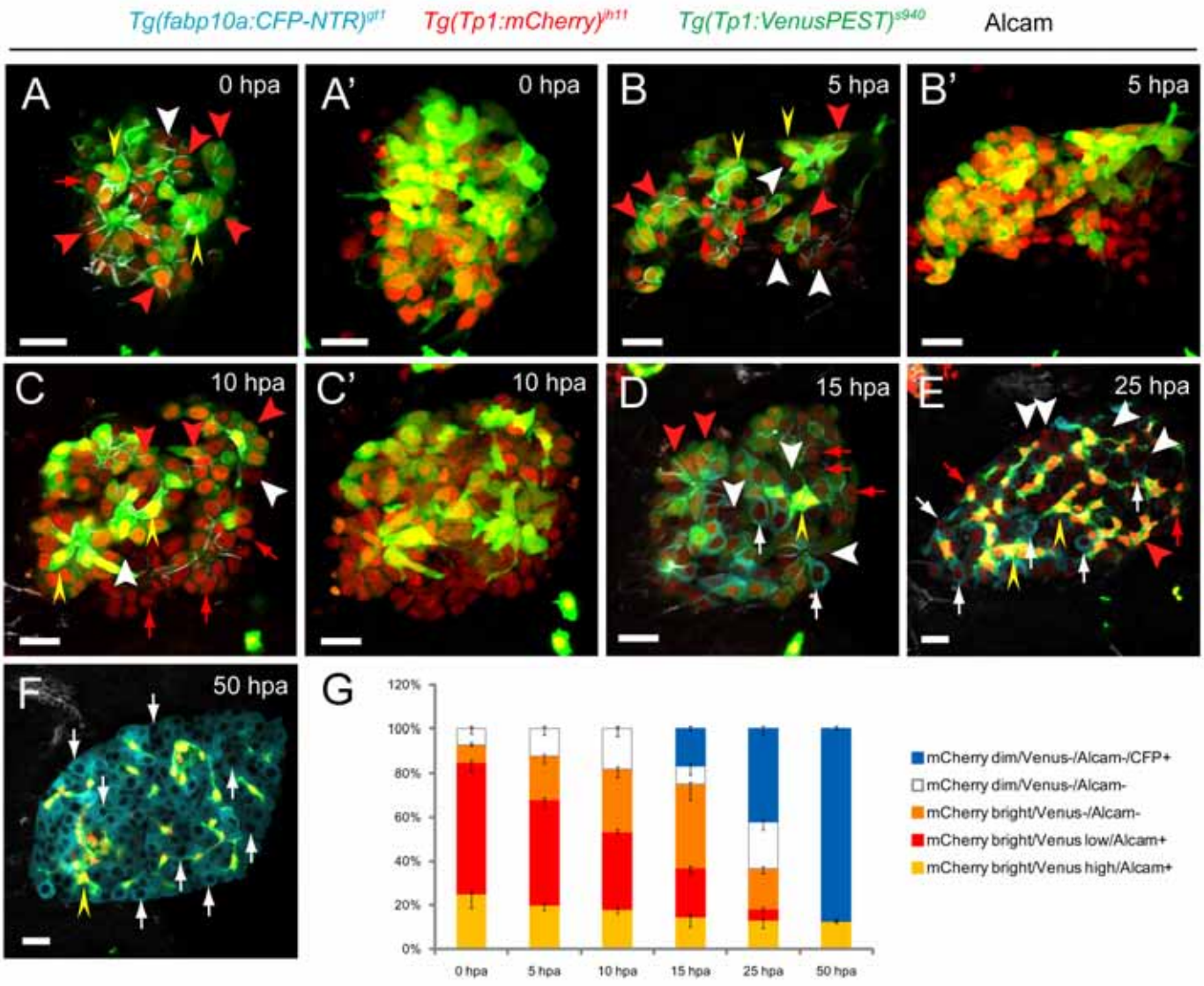

HEP-14-0077
Supporting Fig. 12

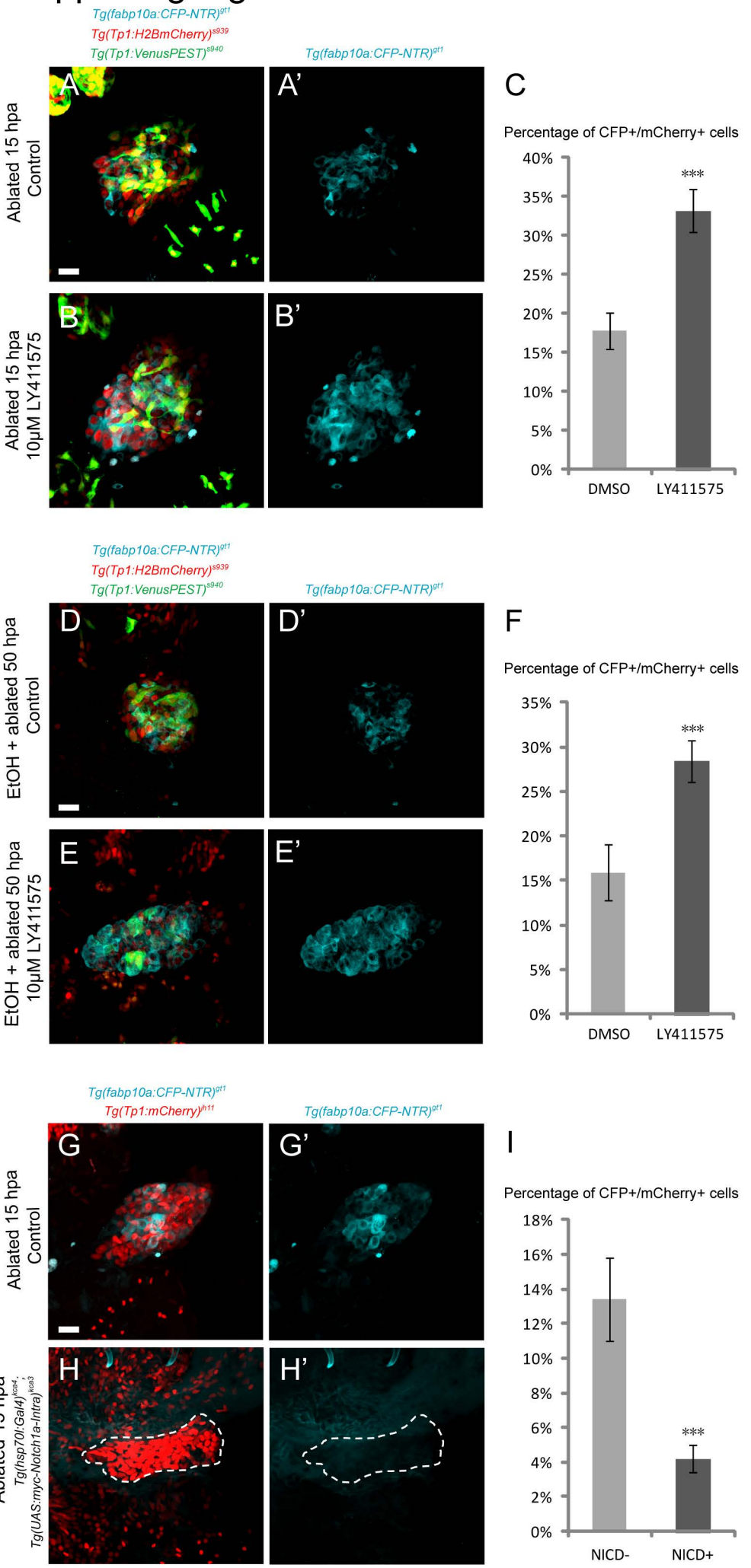

HEP-14-0077
Supporting Fig. 13

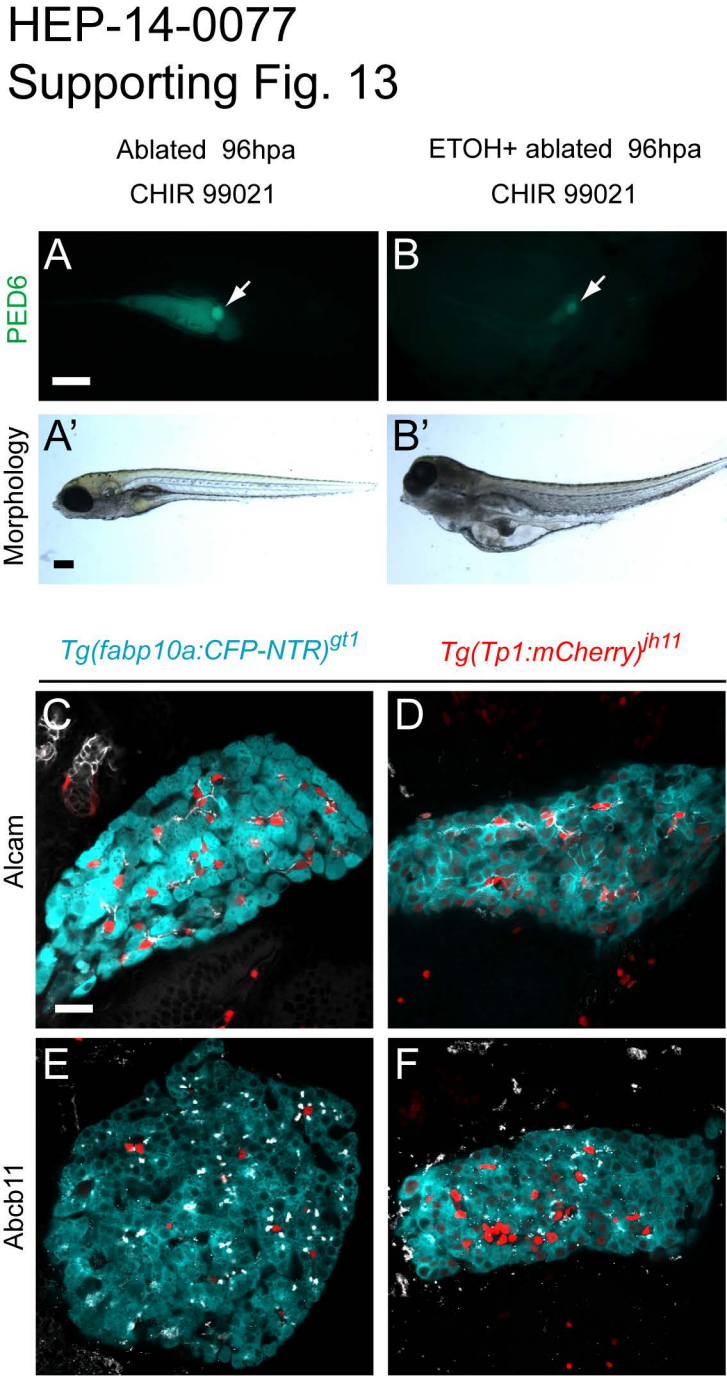

HEP-14-0077
Supporting Fig. 14